Nov 4th, 12:00 AM - Nov 5th, 12:00 AM

Behavior of Complex Hat Shapes Used As Truss Chord Members

Nuthaporn Nuttayasakul

W. Samuel Easterling

Seventeenth International Specialty Conference on Cold-Formed Steel Structures
Orlando, Florida, U.S.A, November 4-5, 2004

BEHAVIOR OF COMPLEX HAT SHAPES USED AS TRUSS CHORD MEMBERS

Nuthaporn Nuttayasakul[1] and W. Samuel Easterling[2]

ABSTRACT

Cold-formed steel roof truss systems that use complex hat shape members for both top and bottom chord elements are a growing trend in the North America steel framing industry. When designing cold-formed steel sections, a structural engineer typically tries to improve the local buckling behavior of the cold-formed steel elements. The complex hat shape has proven to limit the negative influence of local buckling. However, a distortional buckling mode can be the control mode of failure in the design for the chord member with an intermediate un-braced length. The chord member may be subjected to both bending and compressive load because of the continuity of the top and bottom chord members. These members are not typically braced between each panel point in a truss. Numerical analyses using finite strip and finite element procedures were developed to compare with experimental results. A parametric study on geometric imperfection was also conducted to investigate the factors that affect the ultimate strength behavior of a particular complex hat shape. Better understanding of the flexural behavior of these complex hat shapes is necessary to obtain efficient, safe designs of a truss system. The results of these analyses will be presented in the paper.

[1] Graduate Research Assistant, The Charles E. Via, Jr. Dept of Civil and Environmental Engineering, Virginia Polytechnic Institute and State University, Blacksburg, VA, 24061

[2] Professor and Assistant Department Head, The Charles E. Via, Jr. Dept of Civil and Environmental Engineering, Virginia Polytechnic Institute and State University, Blacksburg, VA, 24061

INTRODUCTION

Extensive research has been conducted on the flexural behavior of cold-formed steel sections. Most of the efforts have been concentrated on laterally braced flexural members. Schafer (2002) collected data from tests performed on laterally braced beams, and used the data to calibrate the Direct Strength Method (DSM). The DSM proves to provide acceptable reliability for predicting the flexural strength of laterally braced flexural member. The laterally un-braced chord member in a roof truss raises the question that the existing improvement in the design can be applied effectively.

Experimental studies on laterally unbraced cold-formed steel flexural members have been very limited. Baur and LaBoube (2001) and Nuttayasakul and Easterling (2003) reported that experimental verification of complex hat shapes from different truss manufacturers revealed that these shapes would experience distortional buckling behavior. The AISI Specifications (AISI 1996, North American 2001) does not explicitly address this issue but refers to this issue at the end of the commentary of section C3.1.2. The experimental studies showed that the current 1996 AISI Specification was found to be unconservative. A finite strip analysis was used to determine the critical buckling stress. This buckling stess can be used in the analytical models proposed by Kwon and Hancock (1992) to predict inelastic buckling moments. The so-called Winter and Hancock curves provided good correlation with the experimental results for the beam with intermediate unbraced lengths of 2 and 4 ft.

A finite strip analysis (Schafer 2002) has been used for the determination of the elastic buckling moment. The yield moment (M_y) is based on the full section modulus and the elastic distortional buckling moment (M_{crd}) is based on the finite strip analysis. A cold-formed flexural member may have an increase in moment capacity resulting from inelastic reserve from postbuckling. Kwon and Hancock (1992) reported experimental results for cold-formed steel channels loaded in compression. The experimental results were compared to the curve proposed by Winter (1968) which can be expressed in term of the inelastic distortional moment capacity (M_{nd}) as

For $\lambda_d \leq 0.673$ $\quad M_{nd} = M_y$ (1.1)

For $\lambda_d > 0.673$

$$M_{nd} = \left(1 - 0.22\left(\frac{M_{crd}}{M_y}\right)^{0.5}\right)\left(\frac{M_{crd}}{M_y}\right)^{0.5} M_y \qquad (1.2)$$

Where $\lambda_d = \sqrt{M_y / M_{crd}}$

M_{crd} = Critical elastic distortional buckling moment

After reviewing the comparison, Kwon and Hancock proposed a modified equation to better fit the experimental data. The Hancock curve can be expressed as

For $\lambda_d \leq 0.561$ $\quad M_{nd} = M_y$ (2.1)

For $\lambda_d > 0.561$

$$M_{nd} = \left(1 - 0.25\left(\frac{M_{crd}}{M_y}\right)^{0.6}\right)\left(\frac{M_{crd}}{M_y}\right)^{0.6} M_y \qquad (2.2)$$

EXPERIMENTAL STUDY

The objective of this study is the verification of the flexural behavior of cold-formed steel chord members with the finite element and finite strip methods. The complex hat shape was tested with two different thicknesses and four different geometries. The test set-up was a four-point bending test as shown in Fig. 1. The lateral braces were provided at each load point (Pt) by two-inch flat plates. The hydraulic rams were placed at both ends under the pinned end supports. Load cells were placed at both ends of the unbraced length (b), which were either 30 or 60 in. The end length (a) of 20 in. was used for all tests. The hollow structural sections (HSS) were used to simulate the web member of the truss at the end of un-braced length (b). The HSS sections are screwed to the center of the chord member using number 10 self-drilling screws. Table 1 and Figure 2 summarize the geometric properties of the tested specimens.

FINITE ELEMENT ANALYSIS

Numerical models were developed to investigate the full range of parameters not covered by the tests. Finite element models of the cold-formed steel complex hat shape members were developed and validated. The finite element model was developed using the commercial finite element software ABAQUS (Hibbitt et al., 1998). The cold-formed steel member was discretized using element S4R from the ABAQUS finite element library. Element S4R is a four-node, general-purpose shell element with finite strain capability (Hibbitt et al., 1998).

VALIDATION OF FINITE ELEMENT MODEL

The three-dimensional finite element model of the full-scale specimen was created to simulate the test set-up as shown in Fig. 2. A classical eigenvalue buckling analysis and inelastic postbuckling analysis can be performed for this type of problem. In a classical eigenvalue buckling problem, the analysis will estimate the critical buckling loads as well as useful estimates of collapse mode shapes. The collapse mode shapes could be used to introduce an initial imperfection in the postbuckling analysis (Hibbitt et al., 1998). In the postbuckling analysis, ABAQUS employs the Riks method to perform a load-displacement analysis where other important nonlinear effects, such as material inelasticity or degree of imperfection, can be included.

The end boundary conditions of the model are pinned or roller type. The lateral brace boundary conditions were applied to the model at both ends and the ends of unbraced length. In the experiment, the lateral braces were provided at each load points by two-inch flat plates. For material nonlinearity, the nominal stress-strain data were from coupon tests of the specimens as shown in Fig 3, were converted to the true stress and logarithmic plastic strain and used as an input (Hibbitt et al., 1998).

The typical failure mode of the 30 in. and 60 in. unbraced length tests was the first distortional buckling mode shape as shown in Fig. 4. The shape of the first mode failure from the FEM analyses agrees with the tests and is the same for all the analyses. The shapes of the second mode failure are different depending on the thickness and the unbraced length as shown in Table 2 and Fig. 4. Each of the 3x5 ga14 and ga22 tests at a 30 in. unbraced length, exhibited a second mode Type I failure, as illustrated in Fig 4. The failure in the second mode could occur because of the initial imperfection of the tested specimen.

The results of the elastic FEM are summarized in Table 3. The FEM results show good comparison with the average from the test results. The elastic buckling loads (Pt) from both first and second mode are calculated because the second mode failures occurred as mentioned earlier. The elastic FEM results are conservative when compared to the average value of the tests.

The CFS software (1998) was used to calculate the moment capacity, $M_{n,\ AISI}$, according to the 1996 AISI Specification (Specification, 1996). All calculations were based on the yield stress from tensile coupon tests. The prediction of the inelastic distortional buckling moment capacity, M_{nd}, using both Winter's and Hancock's equations were also calculated. The CUFSM software (Schafer, 2002) was used to generate the elastic buckling curve to determine the elastic distortional moment, M_{crd}, as an input to equation 1 and 2.

As a result, five predictions (from the 1996 AISI Specification, the Winter equation, the Hancock equation, classical eigenvalue buckling FEM results, and inelastic postbuckling FEM results) were compared with the experimental results as shown in Table 4 and 5. The results in Table 4 and 5 show the ratio between the test moment and predicted moment for 30 in. and 60 in. unbraced lengths, respectively. The ratios of the test results over the moment capacity predicted by the 1996 AISI Specification for 22-gage specimen is found to be as low as 0.44 and 0.56 for the 30 in. and 60 in. unbraced length tests, respectively. This result shows that the 1996 AISI Specification is unconservative in predicting the flexural behavior at this intermediate length.

The statistical analyses of these comparisons can be used to better analyze the test results. The mean, standard deviation, coefficient of variation, and resistance factor (Φ) of the comparison ratios are also tabulated in Table 4 and 5. The resistance factors were calculated based on the reliability index (β) of 2.5 according the 1996 AISI Specification. Both elastic FEM and postbuckling FEM analyses yield more reliable values when compared with other methods. The mean values of postbuckling FEM comparison with the tests are 1.10 and 1.26 and the resistance factors (Φ) are the highest at 0.84 and 0.87 for the 30 in. and 60 in. unbraced length tests, respectively.

PARAMETRIC STUDY

The effect of geometric imperfections on strength was evaluated through a parametric study. Schafer and Pekoz (1997) recommended the use of a maximum deviation that is approximately equal to the plate thickness as a

simple rule of thumb. In this study, the maximum deviations of the perturbed initial imperfection from the perfect geometry are at 10%, 100%, and 150% of the plate thickness. The buckling shapes of Mode I and Mode II are used in the postbuckling analyses to determine the load-displacement curve and the maximum loads are reported in Table 6.

From the results, the typical plots of the geometric imperfection study can be shown in Fig. 5 and 6. Depending on the initial geometric imperfection, mode II ultimate failure could be approximately close to those of mode I with larger initial geometric imperfection. These plots help explain why there were second mode failures in the test of the 3x5 specimens.

The geometric imperfection tends to have little effect on the strength of the specimen with 22 ga material at the unbraced length of 60 in. The same trend also applies to the specimen with 22 ga material at the unbraced length of 30 in. for 3x3.5 and 2.5x3.5 specimens. These specimens have smaller width to thickness ratios than the others where the geometric imperfection yields greater effect on their strength. In another words, the specimens that tend to fail in a distortional buckling mode tend to be more sensitive to geometric imperfection. These specimens are those with unbraced lengths of 30 in. and have high width to thickness ratios.

Another interesting observation from the postbuckling analyses of the second mode shape is the analysis of type II as shown in Fig. 4. When imposing the geometric imperfection of the second mode type II on the perfect geometry, some of the analyses, especially the one with 150%t imperfection, ultimately failed in the first mode failure. The final failure of the postbuckling analyses turned out to be the first mode failure even when the initial geometric imperfection was imposed as the second mode type II.

CONCLUSIONS

The comparisons of the experimental results with the predictions from the 1996 AISI Specification yield unconservative values and are less reliable compared to the predictions by Winter, Hancock, and FEM, especially with the 22-gage specimen. Both elastic FEM and postbuckling FEM analyses yield more reliable values when compared with other methods. The resistance factors (Φ) from the post buckling FEM are the highest at 0.84 and 0.87 for the 30 in. and 60 in. unbraced length tests, respectively. The parametric study on the

geometric imperfection also shows that the geometric imperfection can have significant effect on the strength and the failure mode shape.

REFERENCES

Baur, S.W. and LaBoube, R.A. (2001), "Behavior of Complex Hat Shape Cold-Formed Steel Members", *Proceedings of Structural Stability Research Council*, University of Missouri-Rolla, 403-417.

CFS Cold-formed Steel Design Software, (1998), Version 3.0, RGS Software, Inc. 2803 NW Chipman Road Lee's Summit, MO.

Hibbitt, Karlsson and Sorensen, 1998. ABAQUS/Users Manual. Hibbitt, Karlsson and Sorensen Inc., Pawtucket, RI.

Kwon, Y.B. and Hancock, G.J. (1992), "Strength Tests of Cold-Formed Channel Sections Undergoing Local and Distortional Buckling", ASCE *Journal of Structural Engineering*, 118(7).

North American Specification for the Design of Cold-Formed Steel Structural Members (2001), American Iron and Steel Institute, Washington, D.C.

Nuttayasakul, N. and Easterling, W.S. (2003), "Cold-Formed Steel Flexural Members Undergoing Distortional and Euler Buckling", *Proceedings of Structural Stability Research Council*, University of Missouri-Rolla, 339-355.

Specification for the Design of Cold-Formed Steel Structural Members (1996), American Iron and Steel Institute, Washington, D.C.

Schafer, B.W. (2002), "Progress on the Direct Strength Method", *Proceedings 16th Int'l Spec. Conf. on Cold-Formed Steel Structures*, University of Missouri-Rolla, 647-662.

Schafer, B.W. and Pekoz, T. (1998), "Computational modeling of cold-formed steel characterizing geometric imperfections and residual stresses", *Journal of Constructional Steel Research*, 47, 193-210.

Table 1 Geometric Properties of Tested Sections

Designation	Thickness	Nominal Dimension (in.)					Section
	(in.)	A	B	C	D	E	Modulus (in^3)
3.0x5.0-14GA	0.071	3.00	5.00	0.75	0.25	0.50	1.051
3.0x5.0-22GA	0.028	3.00	5.00	0.75	0.25	0.50	0.446
2.5x5.0-14GA	0.071	2.50	5.00	0.75	0.25	0.50	0.831
2.5x5.0-22GA	0.028	2.50	5.00	0.75	0.25	0.50	0.434
3.0x3.5-14GA	0.071	3.00	3.50	0.75	0.25	0.50	0.587
3.0x3.5-22GA	0.028	3.00	3.50	0.75	0.25	0.50	0.253
2.5x3.5-14GA	0.071	2.50	3.50	0.75	0.25	0.50	0.570
2.5x3.5-22GA	0.028	2.50	3.50	0.75	0.25	0.50	0.246

Note: All Inside Bend Radii are 0.125 in.

Table 2 Type of Second Mode Shape

Specimen	GA	Length (in.)	Second Mode Shape (Type)
3.0x5.0	14	30	I
		60	II
	22	30	I
		60	I
2.5x5.0	14	30	I
		60	II
	22	30	I
		60	I
3.0x3.5	14	30	I inverse
		60	II
	22	30	I inverse
		60	II
2.5x3.5	14	30	I inverse
		60	II
	22	30	I inverse
		60	II

Table 3 FEM elastic buckling results

Specimen	GA	Length (in.)	Test Average (lb)	FEM Elastic Buckling	
				Mode I (lb)	Mode II (lb)
3.0x5.0	14	30	1737	1693	1923
		60	1365	1286	1424
	22	30	448	446	461
		60	310	250	310
2.5x5.0	14	30	1900	1593	1926
		60	1213	1099	1357
	22	30	348	427	452
		60	313	231	314
3.0x3.5	14	30	1570	1584	2038
		60	1287	1234	1413
	22	30	403	359	386
		60	313	233	292
2.5x3.5	14	30	1598	1438	2094
		60	1165	946	1240
	22	30	408	337	381
		60	267	204	273

Table 4 Performance Predictions for 30 inches Beams

Specimen	ga	$\frac{M_t}{M_n^{FEM}{}_{el}}$	$\frac{M_t}{M_n^{FEM}{}_{inel}}$	$\frac{M_t}{M_n^{Winter}}$	$\frac{M_t}{M_n^{Hancock}}$	$\frac{M_t}{M_n^{AISI}}$
3.0x5.0	14	0.96	1.00	0.99	1.09	0.63
		1.05	1.10	1.08	1.20	0.70
		0.92	0.95	0.94	1.05	0.61
		1.07	1.11	1.10	1.22	0.71
3.0x5.0	22	1.03	1.06	0.92	1.08	0.57
		1.12	1.15	1.00	1.17	0.62
		0.92	0.94	0.82	0.96	0.51
		1.07	1.09	0.95	1.11	0.59
2.5x5.0	14	1.22	1.26	1.54	1.71	1.04
		1.15	1.19	1.44	1.60	0.98
		1.20	1.24	1.50	1.67	1.02
		1.20	1.24	1.50	1.67	1.02
2.5x5.0	22	0.80	0.82	0.69	0.80	0.45
		0.77	0.80	0.67	0.78	0.44
		0.82	0.84	0.71	0.82	0.46
		0.87	0.89	0.75	0.87	0.49

Table 4 (continued) Performance Predictions for 30 inches Beams

Specimen	ga	$\frac{M_t}{M_n^{FEM}{}_{el}}$	$\frac{M_t}{M_n^{FEM}{}_{inel}}$	$\frac{M_t}{M_n^{Winter}}$	$\frac{M_t}{M_n^{Hancock}}$	$\frac{M_t}{M_n^{AISI}}$
3.0x3.5	14	1.02	1.11	1.34	1.42	1.11
		0.98	1.08	1.30	1.37	1.08
		0.99	1.08	1.31	1.38	1.08
		0.97	1.06	1.28	1.36	1.06
3.0x3.5	22	1.28	1.29	1.21	1.34	0.80
		1.11	1.12	1.06	1.16	0.69
		1.03	1.04	0.98	1.07	0.64
		1.06	1.07	1.00	1.10	0.66
2.5x3.5	14	1.10	1.18	1.39	1.47	1.23
		1.17	1.25	1.48	1.56	1.31
		1.18	1.26	1.48	1.57	1.31
		1.00	1.07	1.27	1.34	1.12
2.5x3.5	22	1.16	1.18	1.04	1.14	0.77
		1.36	1.39	1.23	1.34	0.91
		1.25	1.27	1.12	1.23	0.83
		1.07	1.09	0.96	1.05	0.71
Average		1.059	1.06	1.10	1.13	1.24
Std. Dev.		0.141	0.14	0.14	0.26	0.26
C.O.V.		13.3%	13.0%	23.0%	21.0%	32.2%
Phi		0.84	0.84	0.71	0.74	0.59

Table 5 Performance Predictions for 60 inches Beams

Specimen	ga	$\frac{M_t}{M_n^{FEM}{}_{el}}$	$\frac{M_t}{M_n^{FEM}{}_{inel}}$	$\frac{M_t}{M_n^{Winter}}$	$\frac{M_t}{M_n^{Hancock}}$	$\frac{M_t}{M_n^{AISI}}$
3.0x5.0	14	1.11	1.18	0.93	1.04	0.92
		1.08	1.15	0.90	1.01	0.90
		1.07	1.13	0.89	1.00	0.89
		0.99	1.05	0.82	0.92	0.82
3.0x5.0	22	1.32	1.37	0.75	0.89	0.63
		1.24	1.29	0.70	0.84	0.59
		1.24	1.29	0.70	0.84	0.59
		1.16	1.20	0.66	0.79	0.56
2.5x5.0	14	1.15	1.21	1.16	1.32	1.56
		1.06	1.11	1.06	1.22	1.44
		1.11	1.17	1.12	1.28	1.51
2.5x5.0	22	1.39	1.44	0.77	0.93	0.82
		1.39	1.44	0.77	0.93	0.82
		1.30	1.35	0.73	0.88	0.77

Table 5 (continued) Performance Predictions for 60 inches Beams

Specimen	ga	$\frac{M_t}{M_n^{FEM}{}_{el}}$	$\frac{M_t}{M_n^{FEM}{}_{inel}}$	$\frac{M_t}{M_n^{Winter}}$	$\frac{M_t}{M_n^{Hancock}}$	$\frac{M_t}{M_n^{AISI}}$
3.0x3.5	14	1.06	1.14	1.29	1.41	1.36
		1.07	1.15	1.30	1.42	1.37
		1.00	1.07	1.21	1.32	1.28
3.0x3.5	22	1.33	1.35	0.95	1.08	0.85
		1.29	1.31	0.92	1.04	0.82
		1.55	1.57	1.10	1.25	0.99
		1.20	1.22	0.86	0.97	0.77
2.5x3.5	14	1.29	1.35	1.40	1.55	1.84
		1.22	1.27	1.32	1.47	1.74
		1.24	1.29	1.34	1.49	1.77
		1.18	1.24	1.29	1.43	1.69
2.5x3.5	22	1.37	1.42	0.94	1.08	1.06
		1.23	1.27	0.84	0.97	0.94
		1.32	1.37	0.91	1.05	1.02
Average		1.212	1.21	1.26	0.99	1.12
Std. Dev.		0.134	0.13	0.12	0.23	0.23
C.O.V.		11.1%	9.9%	23.0%	20.5%	36.4%
Phi		0.86	0.87	0.71	0.75	0.54

Table 6 FEM Predictions for First Mode Imperfection

Specimen	GA	Length (in.)	FEM Post Buckling Mode I (lb)		
			10%t	t	150%t
3.0x5.0	14	30	1625	1393	1343
		60	1211	1105	1081
	22	30	435	389	377
		60	241	239	238
2.5x5.0	14	30	1544	1335	1282
		60	1043	973	953
	22	30	415	375	363
		60	222	222	221
3.0x3.5	14	30	1449	1242	1201
		60	1146	1050	1017
	22	30	356	327	314
		60	229	229	227
2.5x3.5	14	30	1343	1152	1102
		60	905	826	797
	22	30	331	306	294
		60	197	194	191

Table 6 (continued) FEM Predictions for Second Mode Imperfection

Specimen	GA	Length (in.)	FEM Post Buckling Mode II (lb)		
			10%t	t	150%t
3.0x5.0	14	30	1886	1688	1654
		60	1415	1205	1178
	22	30	446	414	405
		60	512	335	353
2.5x5.0	14	30	1588	1689	1657
		60	1330	1186	1043
	22	30	444	411	402
		60	363	356	356
3.0x3.5	14	30	1594	1332	1289
		60	1333	1129	1103
	22	30	356	327	322
		60	291	230	229
2.5x3.5	14	30	1452	1333	1287
		60	1191	916	904
	22	30	340	331	315
		60	273	255	198

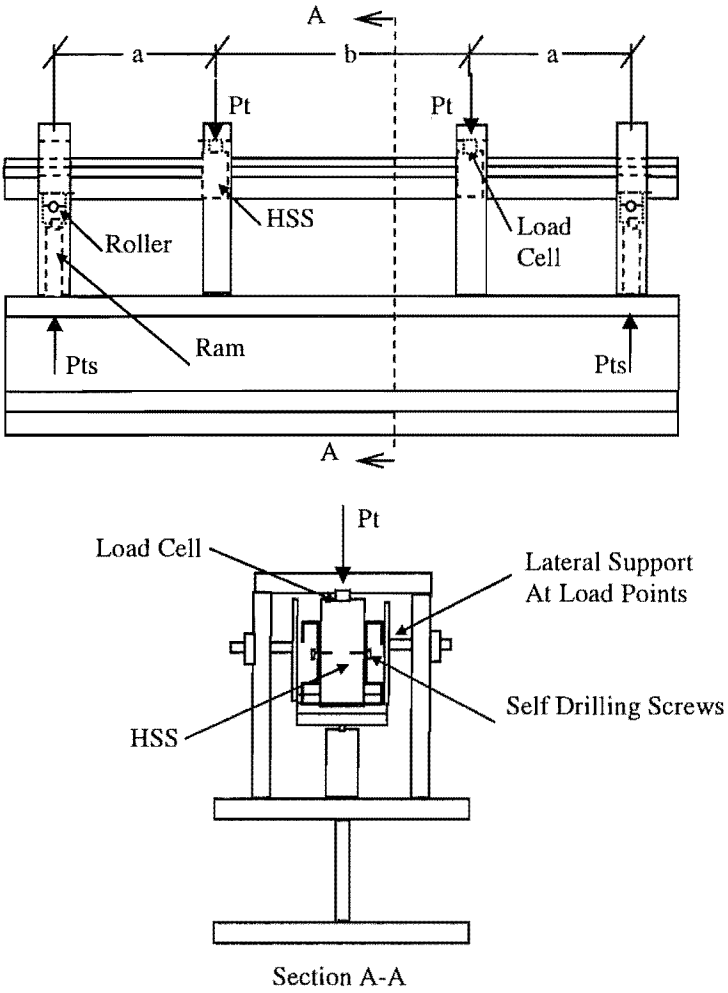

Figure 1 Schematic Drawing of Test Set-up

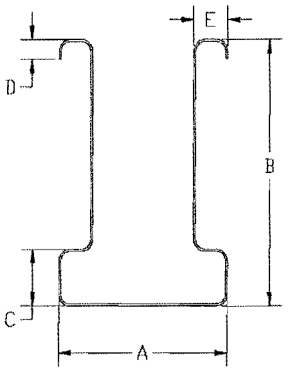

Figure 2 Typical Chord Member Geometry

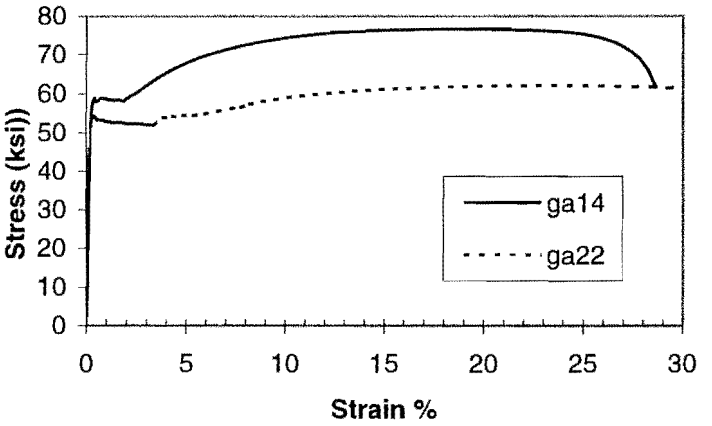

Figure 3 Typical Stress-Strain Curve for FEM

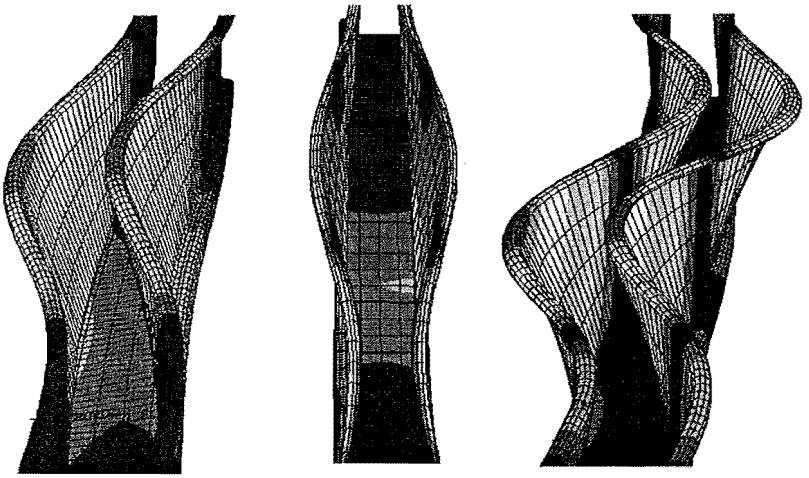

First Mode Second Mode: Type I Type II

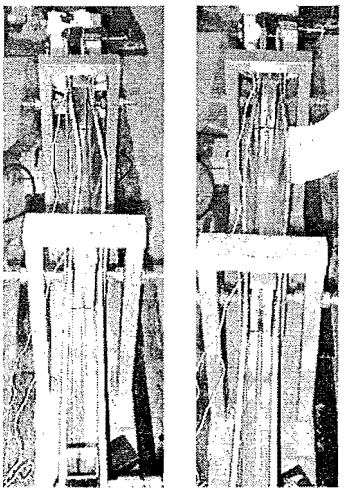

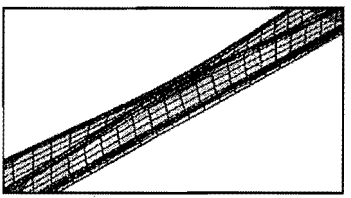

Second Mode: Type I inverse

Figure 4 FEM Mode Shapes and Tests Comparison

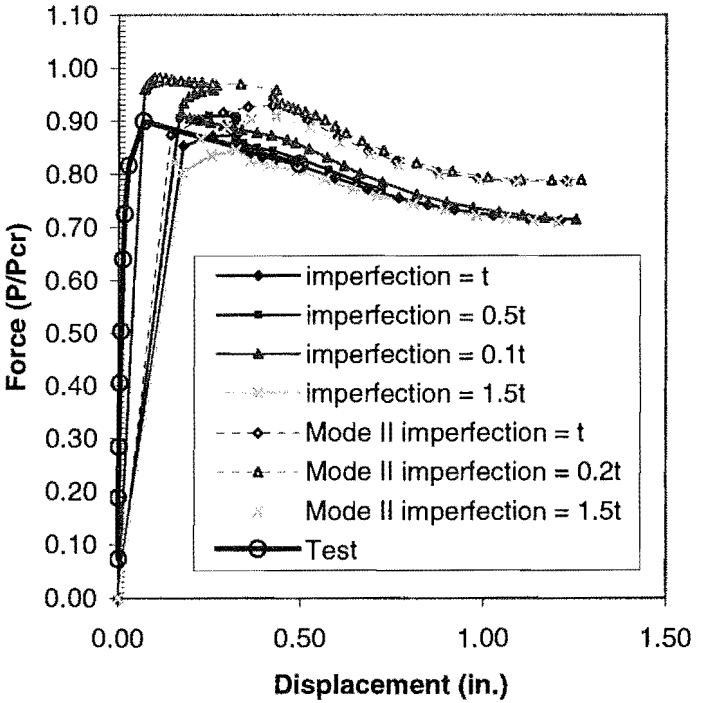

Figure 5 Force vs Displacement Plot of Chord
3x5 ga22 @30 inch

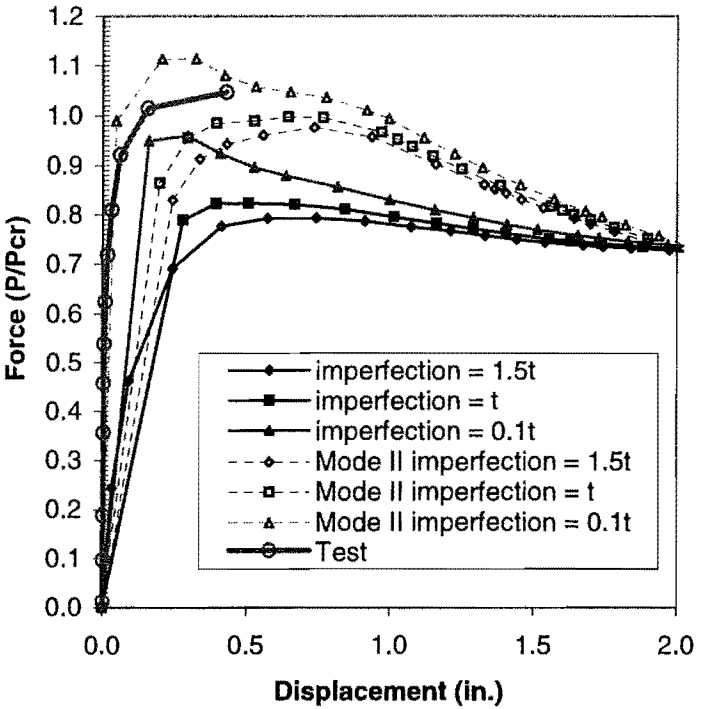

Figure 6 Force vs Displacement Plot of Chord
3x5 ga14 @30 inch